k_z Selective Scattering within Quasiparticle Interference Measurements of FeSe

Luke C. Rhodes,[1,2,3] Matthew D. Watson,[3] Timur K. Kim,[2] and Matthias Eschrig[1,4]
[1]Department of Physics, Royal Holloway, University of London, Egham, Surrey TW20 0EX, United Kingdom
[2]Diamond Light Source, Harwell Campus, Didcot OX11 0DE, United Kingdom
[3]School of Physics and Astronomy, University of St. Andrews, St. Andrews KY16 9SS, United Kingdom
[4]Institute of Physics, University of Greifswald, Felix-Hausdorff-Strasse 6, 17489 Greifswald, Germany

(Received 5 June 2019; revised manuscript received 9 September 2019; published 22 November 2019)

Quasiparticle interference (QPI) provides a wealth of information relating to the electronic structure of a material. However, it is often assumed that this information is constrained to two-dimensional electronic states. We show that this is not necessarily the case. For FeSe, a system dominated by surface defects, we show that it is actually all electronic states with negligible group velocity in the z axis that are contained within the experimental data. By using a three-dimensional tight-binding model of FeSe, fit to photoemission measurements, we directly reproduce the experimental QPI scattering dispersion, within a T-matrix formalism, by including both $k_z = 0$ and $k_z = \pi$ electronic states. This result unifies both tunnelling based and photoemission based experiments on FeSe and highlights the importance of k_z within surface sensitive measurements of QPI.

DOI: 10.1103/PhysRevLett.123.216404

The iron-based superconductor FeSe has recently been a focal point in the study of unconventional superconductivity. The momentum dependence of the superconducting gap, extracted from angle-resolved photoemission spectroscopy (ARPES) [1–5] and quasiparticle interference (QPI) measurements [6,7], has been shown to be highly twofold symmetric, and sensitive to the orbital content of the bands. However, a consensus relating to the full theoretical implications of this gap structure has remained limited due to the range of different, and often contradictory, models of the electronic structure used as a starting point for theoretical investigations [5,6,8–11].

In order to resolve the differences in theoretical models of the electronic structure, it is important to study the results and conclusions extracted from experimental measurements, such as ARPES and QPI. However, there is currently a discrepancy between the interpretation of the data obtained by these two techniques. QPI measurements of FeSe [7,12,13], obtained via scanning tunneling microscopy (STM), have been interpreted as being consistent with a theoretical model where the Fermi surface consists of one hole pocket and two electron pockets and exhibits a large difference in the quasiparticle weight of the d_{xz} and d_{yz} orbitals [13]. On the contrary, the orbital sensitive measurements from ARPES have been interpreted as being consistent with a model with roughly equivalent quasiparticle weights for the d_{xz} and d_{yz} orbitals [3,5,14,15], but with only one hole pocket and one electron pocket at the Fermi surface [16–18]. Interestingly, both of these interpretations have been used to correctly describe the momentum dependence of the superconducting gap [5,8], yet they completely contradict one another on the topology and orbital coherence of the electronic structure.

In this Letter, we address this discrepancy. We show that the ARPES-based interpretation of the electronic structure, i.e., a model which has equal quasiparticle weights for all orbitals but has only one hole pocket and one electron pocket at the Fermi level, is fully consistent with the QPI measurements of FeSe, once all electronic scattering vectors which exhibit zero Fermi velocity in the k_z axis are taken into account. This result therefore provides experimental unification of the electronic structure of FeSe, as determined by ARPES and STM, and highlights the importance of k_z within the surface sensitive measurements of QPI.

Methodology.—QPI is the phenomenon which occurs when propagating quasiparticles scatter elastically from a local potential caused by an impurity, leading to interference patterns in the local density of states. This effect is observable in STM measurements as oscillations in the spatial dependence of the tunneling current emanating from a defect or vacancy. The Fourier transform of these oscillations then unveils a momentum- and energy-dependent structure that may be interpreted in terms of scattering processes, $\mathbf{q} = \mathbf{k} - \mathbf{k}'$, where the momenta $\mathbf{k}$ and $\mathbf{k}'$ are defined by the underlying single particle electronic structure. However, it is important to note that the information obtained from this two-dimensional Fourier transform comes from measurements which, in real space, are restricted to tunneling from the topmost layer of the material. As a consequence, for defects located in the surface layer of a material, which is the dominant form of impurities in FeSe [6], this imposes a restriction: Any coherent oscillations detected far

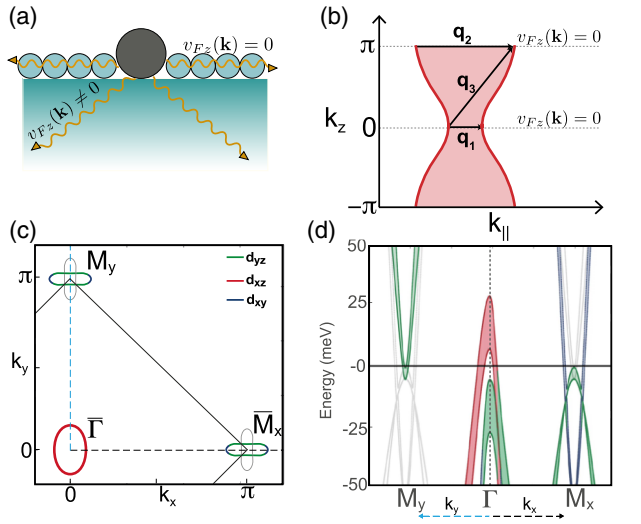

FIG. 1. (a) Electron propagation from a surface defect, STM is sensitive only to the topmost layer of the material; therefore, only QPI arising from the electronic states with $v_{Fz}(\mathbf{k}) = 0$ (orange arrows) will be detected via STM. (b) Cut of the k_z dispersion of the hole pocket of FeSe, highlighting states where $v_{Fz}(\mathbf{k}) = 0$. This then leads to three sets of scattering vectors with unique k_z dependence, labeled as $\mathbf{q_1}, \mathbf{q_2}, \mathbf{q_3}$. This description equivalently holds for the electron pocket and interpocket scattering. (c) Fermi surface of the ARPES-based model of FeSe at $k_z = \pi$. The black line describes the Brillouin zone boundary. (d) Band dispersion along $\bar{M}_y - \bar{\Gamma} - \bar{M}_x$ with projected k_z states. The solid lines describe the $k_z = 0$ and $k_z = \pi$ states, whereas the shaded regions indicate states with intermediate k_z. The gray bands show the states that we have manually excluded from the calculation in order to reproduce ARPES measurements [16].

away from a defect must arise from electronic states which have a vanishing group velocity in the z axis. We illustrate this principle in Fig. 1(a).

This condition restricts the detectable scattering processes, to electronic states where both $\mathbf{k}$ and $\mathbf{k}'$ have zero Fermi velocity along the k_z axis [19,20], which, in the case of FeSe, is true for both the $k_z = 0$ and $k_z = \pi$ states. Thus, there should be three sets of scattering vectors, labeled as $\mathbf{q_1}, \mathbf{q_2}$, and $\mathbf{q_3}$ in Fig. 1(b), which will produce detectable QPI within STM measurements. Previous QPI calculations of FeSe have included the $k_z = 0$ to $k_z = 0$ set of scattering vectors ($\mathbf{q_1}$) [13,21] but have neglected the contributions from $\mathbf{q_2}$ and $\mathbf{q_3}$. In this Letter, we include all three sets of $\mathbf{q}$ vectors within the typical T-matrix calculation of the local density of state [LDOS; $N(\mathbf{q}, \omega)$] [22], where the summation over both k_z and q_z are constrained to the 0 or π plane and the total LDOS is then the sum of the three sets of $\mathbf{q}$ vectors,

$$\tilde{N}(q_x, q_y, \omega) = \sum_{q_z \in [0,\pi]} N(q_x, q_y, q_z, \omega). \tag{1}$$

We note that Eq. (1) is calculated assuming bulk QPI scattering. Formally, open boundary conditions in the z axis should be used to describe the surface of a material [23]; however, as no surface states have been detected for FeSe [24], Eq. (1) is still a valid approximation, which, as we will show, accurately describes the experimental data.

In order to facilitate a comparison between theory and experimental data, we next calculate the normalized LDOS, $L(\mathbf{r}, \omega)$, also referred to as the Feenstra function [25],

$$L(\mathbf{r}, \omega) = \frac{\tilde{N}(\mathbf{r}, \omega)}{\sum_{\omega'=0}^{\omega'=\omega} \tilde{N}(\mathbf{r}, \omega')}. \tag{2}$$

Here, $\tilde{N}(\mathbf{r}, \omega)$ is the 2D inverse Fourier transform of Eq. (1). We then plot the Fourier transform of $L(\mathbf{r}, \omega)$, in moment space, and directly compare our results with the QPI data from Ref. [7].

To calculate Eq. (2), we employ a tight-binding model which has been optimized to describe the band dispersions determined from ARPES measurements of detwinned crystals of FeSe [16]. In Ref. [16], it was observed that, at low temperatures, the Fermi surface of FeSe consisted of one hole pocket and a single electron pocket. However, tight-binding models of FeSe suggest that two electron pockets should be present at the Fermi surface [26]. To account for this experimental observation, we have chosen to specifically exclude bands associated with this unobserved second electron pocket. These bands are shown in gray in Figs. 1(c) and 1(d). To exclude these bands, we use the unfolded one-Fe unit cell of FeSe, which separates the electron pockets in momentum space [27,28]. We then employ a Green's function,

$$\hat{G}_0(\mathbf{k}, \omega) = \frac{1}{[\omega + i\Gamma(\mathbf{k})]\hat{1} - \hat{H}^0(\mathbf{k})}, \tag{3}$$

that includes a momentum-dependent broadening parameter, $\Gamma(\mathbf{k})$. We define $\Gamma(\mathbf{k})$ as arbitrarily large (>100 eV) in the vicinity of $\mathbf{k} = (0, \pi)$, where our tight-binding model incorrectly describes the presence of a second electron pocket. For all other momenta, we set $\Gamma(\mathbf{k})$ to 1.25 meV. The Hamiltonian, $\hat{H}^0(\mathbf{k})$, then describes hopping between all five d orbitals in the presence of spin orbit coupling. This is discussed in detail in Refs. [5,29]. In this Letter, we have additionally reduced the contribution of spin orbit coupling at the M point to improve the agreement of the band positions at negative energies. To do this, we have reduced the spin orbit coupling strength of the l_x and l_y components to $\lambda_{x/y} = 5$ meV. λ_z is then set to 19 meV. This form of the spin orbit coupling matrix is defined in Ref. [30]. The removal of states "by hand" makes this model highly phenomenological; however, within the energy region of ± 50 meV, this approach quantitatively reproduces the experimental band dispersions measured by ARPES experiments on detwinned crystals [16–18].

Results.—In Fig. 2, we show the impact of including all electronic states with $v_{Fz}(\mathbf{k}) = 0$ within the modeled QPI dispersions. In Figs. 2(a)–2(c), we present the calculated result for a $k_z = 0$ model of FeSe at negative energies. Here, the scattering vectors are dominated by the elliptical outer hole band, which decreases in radius as the energy approaches the Fermi level. When all states with $v_F(z) = 0$ are included, however [shown in Figs. 2(g)–2(i)], the intensity of the scattering vectors associated with the $k_z = 0$ hole band is suppressed. Conversely, the intensity from the scattering vectors associated with the two-dimensional bands around the M point is enhanced. This results in a highly anisotropic scattering dispersion, parallel to the q_x axis, which is in very good agreement with the experimental results of Ref. [7], shown in Figs. 2(m)–2(o). In fact, all of the scattering vectors observed at these energies are accounted for, with the exception of the central scattering vector in Fig. 2(n), which is likely a limitation of our tight-binding parametrization.

Direct agreement between theory and experiment can also be found at positive energies. The $k_z = 0$ model of FeSe exhibits a hole band maximum at +7 meV [2,3,31]. This means that, for energies greater than +7 meV, only a single elliptical electron band will contribute to the scattering dispersion in our model. This is shown in Figs. 2(d)–2(f). Scattering vectors arising from the $k_z = 0$ hole band can be observed in Fig. 2(d), at $\omega = +6$ meV; however, for $\omega = +15$ and +24 meV, only an elliptical dispersion from the electron band is observed. Alternatively, at $k_z = \pi$, the hole band captured within the model has a maximum value of +27 meV. Thus, the inclusion of $k_z = \pi$ electronic states [via the inclusion of $\mathbf{q_2}$ and $\mathbf{q_3}$ from Fig. 1(b)] adds scattering dispersions associated with both hole and electron states. This produces the scattering dispersion shown in Figs. 2(j)–2(l), which is in much better agreement with the experimental measurements of Ref. [7], shown in Figs. 2(p)–2(r). In Fig. 2(j), it is noted that the intensity of the scattering vectors appears rotated compared to the experimental measurement of Ref. [7], shown in Fig. 2(p). This intensity difference can arise from anisotropic scattering processes, which are not included in this calculation. However, as the lengths of the scattering vectors are correctly described, we conclude that the QPI measurements of FeSe are sensitive to all electronic states with $v_{Fz}(\mathbf{k}) = 0$.

In Fig. 2, we have obtained very good agreement with the experimental QPI measurements of Ref. [7] on the assumption that the Fermi surface of FeSe consists of one hole pocket and one electron pocket, as determined by ARPES studies on detwinned crystals [16–18]. However, as discussed previously, *ab initio* calculations [15,32] and most theoretical models of FeSe suggest that the Fermi surface should consist of one hole pocket and two electron pockets. To further support the one-electron-pocket

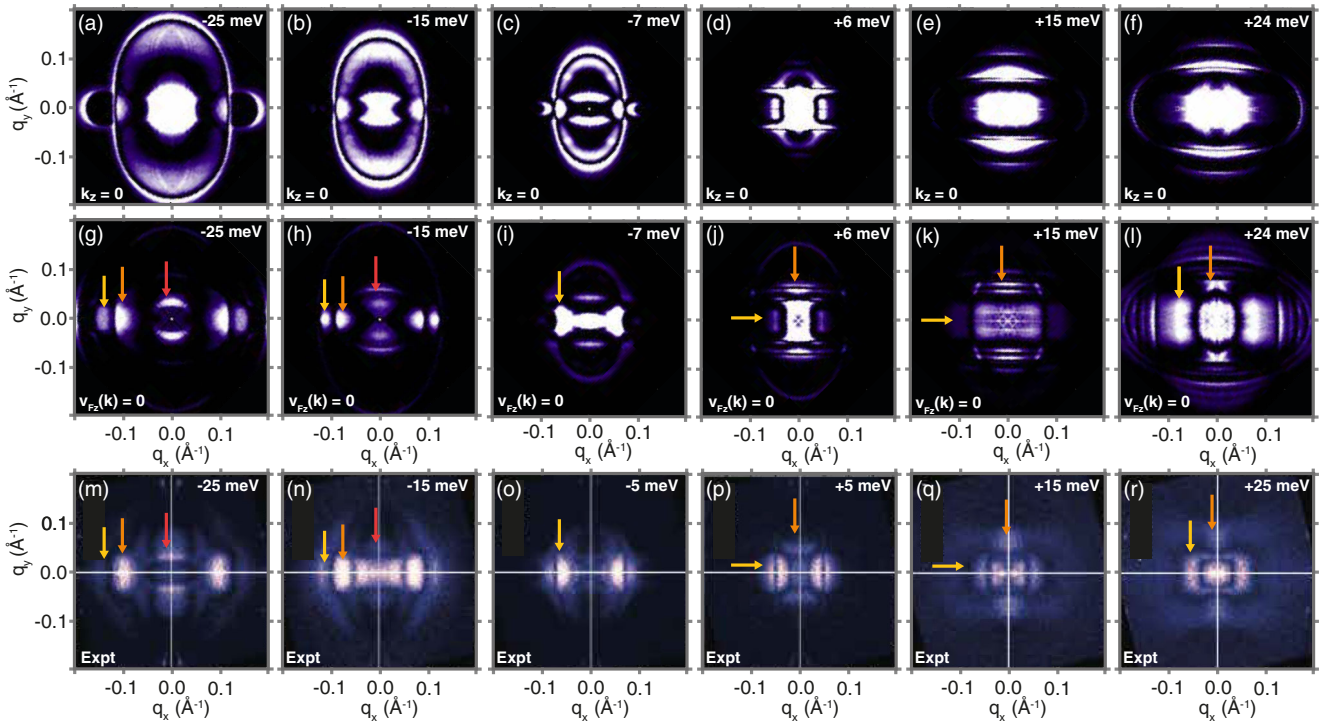

FIG. 2. (a)–(f) Calculated Feenstra function, $|L(\mathbf{q}, \omega)|$ for a two-dimensional, $k_z = 0$ model of FeSe at various energies. (g)–(i) Equivalent calculations for a model of FeSe which includes both $k_z = 0$ and $k_z = \pi$ states. (m)–(r) Experimental QPI data, adapted from Ref. [7] under the Creative Commons Attribution 4.0 International License. The arrows highlight features which are observed in the experimental data and captured within this theoretical framework.

scenario of FeSe, we now focus on the band dispersions determined from QPI. If we include both electron pockets in the calculation, by including the bands shown in gray in Fig. 1(c), we find that the QPI derived band dispersions along the q_x and q_y axes are predicted to be very similar, as shown in Figs. 3(a) and 3(b). In particular, the two-electron-pocket scenario predicts electronlike dispersions in both the q_x and q_y directions. This is in stark contrast to the experimental measurements of Ref. [7], shown in Figs. 3(e) and 3(f), where electronlike dispersions are observed only along the q_y axis. When we repeat this calculation using the one-electron-pocket model of FeSe, shown in Figs. 3(c) and 3(d), we indeed correctly reproduce this anisotropic scattering dispersion, with electronlike dispersions present only along the q_y axis. Moreover, below the Fermi level, in the one-electron-pocket model, more holelike bands are predicted to disperse along the q_x axis than the q_y axis, which is exactly what is observed in the experimental measurements of Figs. 3(e) and 3(f). From this, we conclude that QPI measurements are in agreement with the electronic structure determined by ARPES measurements, where only one electron pocket is detected at the Fermi surface.

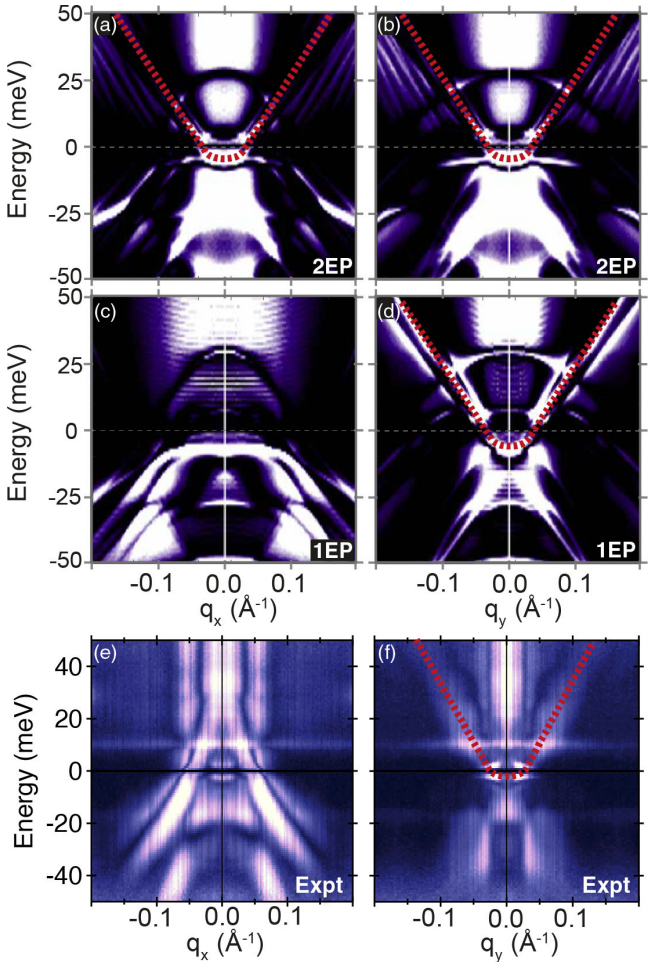

FIG. 3. Energy vs momentum QPI-based band dispersions. (a), (b) QPI band dispersions along q_x at $q_y = 0$ and q_y at $q_x = 0$ for a "two-electron-pocket" (2EP) model of FeSe. The dashed red line highlights electronlike dispersions. (c),(d) Equivalent QPI band dispersion for a "one-electron-pocket" (1EP) model. (e),(f) Experimental QPI band dispersions, adapted from Ref. [7] under the Creative Commons Attribution 4.0 International License.

Discussion.—The importance of including k_z within the analysis of QPI measurements have previously been highlighted in other materials such as $CeCoIn_5$ [33,34] and LiFeAs [35,36]. In this Letter, we have shown that the experimental limitations of STM actually provide a strong selection criteria for the specific values of k_z which can be detected in QPI measurements. Whilst we have focused on the case of FeSe, the conclusions and methodology presented here may be generalised to other three-dimensional materials, which can further improve the agreement between QPI measurements and theoretical models of the electronic structure.

There is great current interest in the fate of the second electron pocket of FeSe, which is predicted to exist within the nematic phase [26,37] but is mysteriously not observed by ARPES at low temperatures [16–18]. Recently, it has been proposed that this missing electron band is actually pushed above the Fermi level, driven by a particular hybridization scheme at the zone boundary in the nematic phase [17,18]. However, in our understanding, the QPI data do not support this interpretation; there is no band minimum observed above the Fermi level, and no low-q electronlike dispersions in the q_x direction [Fig. 3(e)]. Another proposition is that the apparent absence of spectral weight on the second electron pocket is a manifestation of orbital-selective quasiparticle weights [13] since the phenomenological suppression of d_{xz} and d_{xy} weight would particularly affect this pocket. In the Supplemental Material [22], we present simulations including the quasiparticle weight factors suggested in Ref. [13]. We find that, although this approach does account for the general observation of highly twofold symmetric QPI dispersion and qualitatively captures some features, a more satisfactory agreement can be found within our approach, in which we keep all of the orbitals coherent but implement a pocket-selective coherence.

In this Letter, our approach has been to take the ARPES data at face value, and thus to phenomenologically exclude the second electron pocket, and its associated bands, despite the fact that they are present in any reasonable tight-binding model of FeSe. Under this assumption, our simulations correctly reproduce many features of the QPI data, which is not the case when the second electron pocket is included. Thus, this technique, which is independent and complementary to that of ARPES, seems to also indicate the presence of only one electron pocket at the Fermi surface of FeSe. Previously, we have argued that the one-electron-pocket scenario can also naturally account for the

observed superconducting gap structure of FeSe [5], which has been further supported by specific heat measurements [38]. There is, therefore, mounting experimental support for the one-electron-pocket scenario of FeSe, which calls for further theoretical and experimental investigations to elucidate the origin of this effect.

We thank T. Hanaguri for his insight and for providing high quality images of previously published experimental data [7] for comparison with this work. We would also like to thank A. V. Chubukov, A. I. Coldea, A. A. Haghighirad, P. D. C. King, M. van Schilfgaarde, C. Trainer, P. Wahl, M. Yi, and C. M. Yim for the useful discussions.

[1] H. C. Xu, X. H. Niu, D. F. Xu, J. Jiang, Q. Yao, Q. Y. Chen, Q. Song, M. Abdel-Hafiez, D. A. Chareev, A. N. Vasiliev, Q. S. Wang, H. L. Wo, J. Zhao, R. Peng, and D. L. Feng, Highly Anisotropic and Twofold Symmetric Superconducting Gap in Nematically Ordered $FeSe_{0.93}S_{0.07}$, Phys. Rev. Lett. **117**, 157003 (2016).

[2] T. Hashimoto, Y. Ota, H. Q. Yamamoto, Y. Suzuki, T. Shimojima, S. Watanabe, C. Chen, S. Kasahara, Y. Matsuda, T. Shibauchi, K. Okazaki, and S. Shin, Superconducting gap anisotropy sensitive to nematic domains in FeSe, Nat. Commun. **9**, 282 (2018).

[3] D. Liu *et al.*, Orbital Origin of Extremely Anisotropic Superconducting Gap in Nematic Phase of FeSe Superconductor, Phys. Rev. X **8**, 031033 (2018).

[4] Y. S. Kushnirenko, A. V. Fedorov, E. Haubold, S. Thirupathaiah, T. Wolf, S. Aswartham, I. Morozov, T. K. Kim, B. Büchner, and S. V. Borisenko, Three-dimensional superconducting gap in FeSe from angle-resolved photoemission spectroscopy, Phys. Rev. B **97**, 180501(R) (2018).

[5] L. C. Rhodes, M. D. Watson, A. A. Haghighirad, D. V. Evtushinsky, M. Eschrig, and T. K. Kim, Scaling of the superconducting gap with orbital character in FeSe, Phys. Rev. B **98**, 180503(R) (2018).

[6] P. O. Sprau, A. Kostin, A. Kreisel, A. E. Böhmer, V. Taufour, P. C. Canfield, S. Mukherjee, P. J. Hirschfeld, B. M. Andersen, and J. C. Séamus Davis, Discovery of orbital-selective cooper pairing in FeSe, Science **357**, 75 (2017).

[7] T. Hanaguri, K. Iwaya, Y. Kohsaka, T. Machida, T. Watashige, S. Kasahara, T. Shibauchi, and Y. Matsuda, Two distinct superconducting pairing states divided by the nematic end point in $FeSe_{1-x}S_x$, Sci. Adv. **4**, eaar6419 (2018).

[8] A. Kreisel, B. M. Andersen, P. O. Sprau, A. Kostin, D. J. C. Séamus Davis, and P. J. Hirschfeld, Orbital selective pairing and gap structures of iron-based superconductors, Phys. Rev. B **95**, 174504 (2017).

[9] L. Benfatto, B. Valenzuela, and L. Fanfarillo, Nematic pairing from orbital selective spin fluctuations in FeSe, npj Quantum Mater. **3**, 56 (2018).

[10] J. Kang, R. M. Fernandes, and A. Chubukov, Superconductivity in FeSe: The Role of Nematic Order, Phys. Rev. Lett. **120**, 267001 (2018).

[11] H. Hu, R. Yu, E. M. Nica, J. X. Zhu, and Q. Si, Orbital-selective superconductivity in the nematic phase of FeSe, Phys. Rev. B **98**, 220503(R) (2018).

[12] S. Kasahara, T. Watashige, T. Hanaguri, Y. Kohsaka, T. Yamashita, Y. Shimoyama, Y. Mizukami, R. Endo, H. Ikeda, K. Aoyama, T. Terashima, S. Uji, T. Wolf, H. von Löhneysen, T. Shibauchi, and Y. Matsuda, Field-induced superconducting phase of FeSe in the BCS-BEC cross-over, Proc. Natl. Acad. Sci. U.S.A. **111**, 16309 (2014).

[13] A. Kostin, P. O. Sprau, A. Kreisel, Y. X. Chong, A. E. Böhmer, P. C. Canfield, P. J. Hirschfeld, B. M. Andersen, and J. C. Séamus Davis, Imaging orbital-selective quasiparticles in the Hund's metal state of FeSe, Nat. Mater. **17**, 869 (2018).

[14] L. Fanfarillo, J. Mansart, P. Toulemonde, H. Cercellier, P. Le Fèvre, F. Bertran, B. Valenzuela, L. Benfatto, and V. Brouet, Orbital-dependent Fermi surface shrinking as a fingerprint of nematicity in FeSe, Phys. Rev. B **94**, 155138 (2016).

[15] A. Fedorov, A. Yaresko, T. K. Kim, E. Kushnirenko, E. Haubold, T. Wolf, M. Hoesch, A. Grueneis, B. Buechner, and S. V. Borisenko, Effect of nematic ordering on electronic structure of FeSe, Sci. Rep. **6**, 36834 (2016).

[16] M. D. Watson, A. A. Haghighirad, L. C. Rhodes, M. Hoesch, and T. K. Kim, Electronic anisotropies revealed by detwinned angle-resolved photo-emission spectroscopy measurements of FeSe, New J. Phys. **19**, 103021 (2017).

[17] M. Yi, Y. Zhang, H. Pfau, T. Chen, Z. R. Ye, M. Hashimoto, R. Yu, Q. Si, D.-H. Lee, P. Dai, Z.-X. Shen, D. H. Lu, and R. J. Birgeneau, The nematic energy scale and missing electron pocket in FeSe, arXiv:1903.04557.

[18] S. S. Huh, J. J. Seo, B. S. Kim, S. H. Cho, J. K. Jung, S. Kim, Y. Y. Koh, C. I. Kwon, J. S. Kim, W. S. Kyung, J. D. Denlinger, Y. H. Kim, B. N. Chae, N. D. Kim, Y. K. Kim, and C. Kim, Lifted electron pocket and reversed orbital occupancy imbalance in FeSe, arXiv:1903.08360.

[19] A. Weismann, M. Wenderoth, S. Lounis, P. Zahn, N. Quaas, R. G. Ulbrich, P. H. Dederichs, and S. Blügel, Seeing the Fermi surface in real space by nanoscale electron focusing, Science **323**, 1190 (2009).

[20] S. Lounis, P. Zahn, A. Weismann, M. Wenderoth, R. G. Ulbrich, I. Mertig, P. H. Dederichs, and S. Blügel, Theory of real space imaging of Fermi surface parts, Phys. Rev. B **83**, 035427 (2011).

[21] D. K. Singh, A. Akbari, and P. Majumdar, Quasi-one-dimensional nanoscale modulation as sign of nematicity in iron pnictides and chalcogenides, Phys. Rev. B **98**, 180506(R) (2018).

[22] See Supplemental Material at http://link.aps.org/supplemental/10.1103/PhysRevLett.123.216404 for details of how $N(\mathbf{q}, \omega)$ is calculated.

[23] T. Zhou, W. Chen, Y. Gao, and Z. D. Wang, Impurity-induced resonant states in topological nodal-line semimetals, arXiv:1905.09185v1.

[24] A. I. Coldea and M. D. Watson, The key ingredients of the electronic structure of FeSe, Annu. Rev. Condens. Matter Phys. **9**, 125 (2018).

[25] R. M. Feenstra, Tunneling spectroscopy of the (110) surface of direct-gap III-V semiconductors, Phys. Rev. B **50**, 4561 (1994).

[26] S. Mukherjee, A. Kreisel, P. J. Hirschfeld, and B. M. Andersen, Model of Electronic Structure and Superconductivity in Orbitally Ordered FeSe, Phys. Rev. Lett. **115**, 026402 (2015).

[27] V. Brouet, M. F. Jensen, P-H. Lin, A. Taleb-Ibrahimi, P. Le Fèvre, F. Bertran, Chia-Hui Lin, Wei Ku, A. Forget, and D. Colson, Impact of the two Fe unit cell on the electronic structure measured by ARPES in iron pnictides, Phys. Rev. B **86**, 075123 (2012).

[28] E. M. Nica, R. Yu, and Q. Si, Glide reflection symmetry, Brillouin zone folding, and superconducting pairing for the $P4/nmm$ space group, Phys. Rev. B **92**, 174520 (2015).

[29] L. C. Rhodes, M. D. Watson, A. A. Haghighirad, M. Eschrig, and T. K. Kim, Strongly enhanced temperature dependence of the chemical potential in FeSe, Phys. Rev. B **95**, 195111 (2017).

[30] T. Saito, Y. Yamakawa, S. Onari, and H. Kontani, Revisit of the orbital-fluctuation-mediated superconductivity in LiFeAs: Nontrivial spin-orbit interaction effects on the bandstructure and superconducting gap function, Phys. Rev. B **92**, 134522 (2015).

[31] M. D. Watson, A. A. Haghighirad, H. Takita, W. Mansur, H. Iwasawa, E. F. Schwier, A. Ino, and M. Hoesch, Shifts and splittings of the hole bands in the nematic phase of FeSe, J. Phys. Soc. Jpn. **86**, 053703 (2017).

[32] H. Eschrig and K. Koepernik, Tight-binding models for the iron-based superconductors, Phys. Rev. B **80**, 104503 (2009).

[33] A. Akbari, P. Thalmeier, and I. Eremin, Quasiparticle interference in the heavy-fermion superconductor $CeCoIn_5$, Phys. Rev. B, **84**, 134505 (2011).

[34] B. B. Zhou, S. Misra, E. H. da Silva Neto, P. Aynajian, R. E. Baumbach, J. D. Thompson, E. D. Bauer, and A. Yazdani, Visualizing nodal heavy fermion superconductivity in $CeCoIn_5$, Nat. Phys. **9**, 474 (2013).

[35] D. Altenfeld, P. J. Hirschfeld, I. I. Mazin, and I. Eremin, Detecting sign-changing superconducting gap in LiFeAs using quasiparticle interference, Phys. Rev. B, **97**, 054519 (2018).

[36] S. Chi, S. Johnston, G. Levy, S. Grothe, R. Szedlak, B. Ludbrook, R. Liang, P. Dosanjh, S. A. Burke, A. Damascelli, D. A. Bonn, W. N. Hardy, and Y. Pennec, Sign inversion in the superconducting order parameter of LiFeAs inferred from Bogoliubov quasiparticle interference, Phys. Rev. B **89**, 104522 (2014).

[37] K. Jiang, J. Hu, H. Ding, and Z. Wang, Interatomic Coulomb interaction and electron nematic bond order in FeSe, Phys. Rev. B **93**, 115138 (2016).

[38] F. Hardy, M. He, L. Wang, T. Wolf, P. Schweiss, M. Merz, M. Barth, P. Adelmann, R. Eder, A. A. Haghighirad, and C. Meingast, Calorimetric evidence of nodal gaps in the nematic superconductor FeSe, Phys. Rev. B **99**, 035157 (2019).